



MODELING OF THE SUBSURFACE STRUCTURE FROM THE SEISMIC BEDROCK TO THE GROUND SURFACE FOR A BROADBAND STRONG MOTION EVALUATION IN KANTO REGION, JAPAN

S. Senna⁽¹⁾, A. Wakai⁽²⁾, A. Yatagai⁽³⁾, H. Suzuki⁽⁴⁾, Y. Inagaki⁽⁵⁾, H. Matsuyama⁽⁶⁾ and H. Fujiwara⁽⁷⁾

⁽³⁾ Principal Researcher, National Research Institute for Earth Science and Disaster Resilience, senna@bosai.go.jp

⁽²⁾ Researcher, National Research Institute for Earth Science and Disaster Resilience, wakai@bosai.go.jp

⁽³⁾ Chief, OYO Corporation, yatagai-atsushi@oyonet.oyo.co.jp

⁽⁴⁾ General Manager, OYO Corporation, suzuki-haruhiko@oyonet.oyo.co.jp

⁽⁵⁾ Deputy General Manager, OYO Corporation, inagaki-yoshiaki@oyonet.oyo.co.jp

⁽⁶⁾ Professional Engineer, OYO Corporation, matsuyama-hisanor@oyonet.oyo.co.jp

⁽⁷⁾ Director, National Research Institute for Earth Science and Disaster Resilience, fujiwara@bosai.go.jp

Abstract

To estimate damage caused by strong ground motions from a large earthquake, it is important to accurately evaluate broadband ground-motion characteristics in wide area. For realizing that, it is one of the important issues to model detailed subsurface structure from top surface of seismic bedrock to ground surface. Here, we focus on Kanto area, including Tokyo, where there are thicker sedimentary layers. We, first, have ever collected deep bore-hole data, soil physical properties obtained by some geophysical explorations, geological information and existing models for deep ground from top surface of seismic bedrock to that of engineering bedrock, and have collected a great number of bore-hole data and surficial geological ones for shallow ground from top surface of engineering bedrock to ground surface. Using them, we modeled initial geological subsurface structure for each of deep ground and shallow one. By connecting them appropriately, we constructed initial geological subsurface structure models from top surface of seismic bedrock to ground surface. In this study, we first collected a lot of records obtained by dense microtremor observations and earthquake ones in the whole area. About microtremor observations, we conducted measurements from large array with the size of hundreds of meters to miniature array with the size of 60 centimeters to cover both of deep ground and shallow one. And then, using ground motion characteristics such as disperse curves and H/V(R/V) spectral ratios obtained from these records, the initial geological subsurface structure models were improved in terms of velocity structure from top surface of seismic bedrock to ground surface in the area. We will report outlines on microtremor array observations, analysis methods and improved subsurface structure models.

Keywords: Microtremors, Borehole, S-wave velocity, Ground motion prediction, 3D velocity structure

1. Introduction

For the improvement of strong ground motion predictions, one of the most important issues is to establish a ground model that can evaluate ground motion characteristics for broadband periods from around 0.1 to 10 seconds. To do this, it is essential to integrate shallow-layer models[1] and deep-layer models[2], which have been modeled separately, and to develop a model that can reproduce observation records. In this study, we first collected boring data of the whole area of each prefecture from municipalities, then we created an initial geological structure model from the earth's surface to the engineering bedrock, and from there the initial



ground model (geologic model) by combining that with the existing deep-layer model²⁾. Next, using this initial ground model as the initial value, we improved the ground model by collecting two sets of records. First, ground motion records in a two-dimensional plane at strong ground motion observation points, such as in K-NET, KiK-net, Japan Meteorological Agency, and municipalities. Then, multiple records of array surveys for microtremors. In addition to that, quantitative data of S-wave velocity structures, correction coefficients (Q-values), and amplification factors also helped to improve the model. Moreover, we examined the two-dimensional interpolation method, and we created a shallow/deep-layers integrated ground model using grids of approximately 250 m. Note that to verify the model for periods shorter than 2 seconds, we compared the model with ground motion records, site amplification factors, and so on, by means of one-dimensional multiple reflection method. For periods longer than 2 seconds, we compared the model with the ground motion records by means of finite-difference method[3]. Then, we examined the accuracy of the model, comparing it with the existing ground models. Finally, to incorporate the seismic response characteristics for the whole Kanto area, we made a map of periods and amplification factors using the one-dimensional multiple reflection method calculated from the ground model with 250-meter grids. Here, we report the efforts to create the model for the Kanto area.

2. Overview of the ground structure modelling

In this study, to create “a broad-area version” of the existing ground model for each prefecture, we examine the method to create “the shallow/deep-layers integrated ground model” using the ground structure models in the existing studies mentioned above, based on a grid unit of about 250 m, which is used also for geomorphologic classification. As of today, we have examined the Kanto/Tokai areas, Niigata Prefecture, and a part of Kumamoto Prefecture (Tokyo and twelve other prefectures) [4,5]. Also, for this examination, we referred to our previous study's shallow/deep-layers integrated ground model and methods⁶⁾, which addressed “local area versions” for each city, town, and village, using a grid size of about 50 m. For the initial shallow/deep-layers integrated ground model, which becomes the initial model and is based on boring data, it is important that the model is made in the same quality for all regions. In this study, by using a three-dimensional stratigraphy as the initial shallow-layer model, we established a ground model where spatial continuity is considered for the whole region except for mountains. Fig-1 shows a schematic diagram of depth used to model the ground in this and other studies, and Fig-2 shows the flow used to make the model.

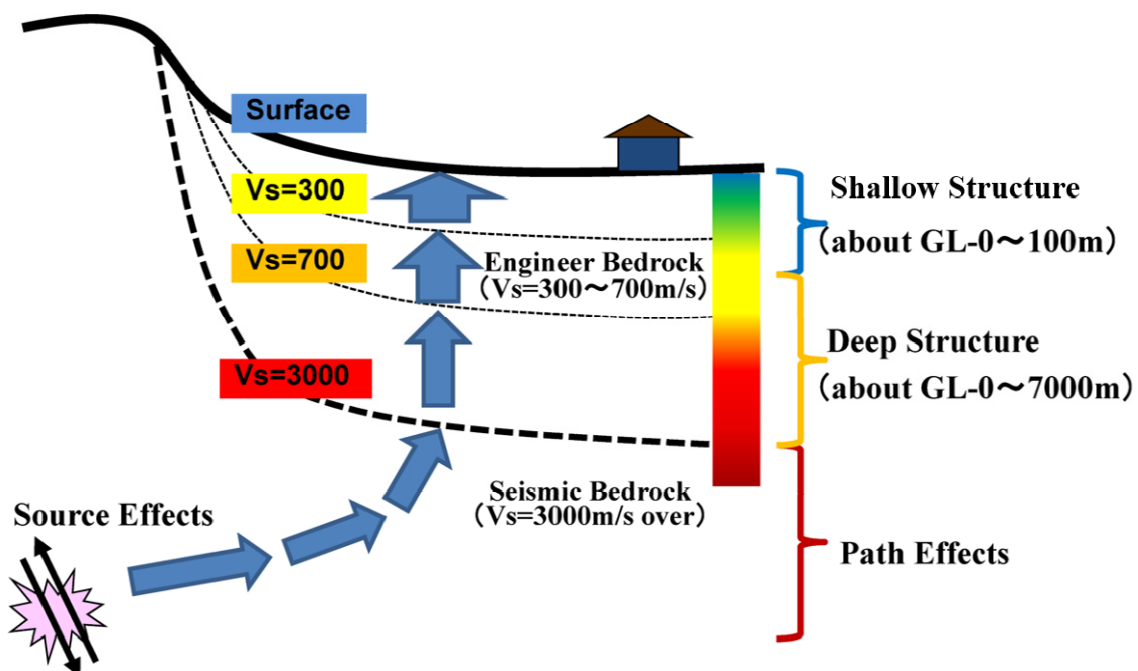


Fig. 1 – Schematic diagram of the range of the subsurface structure model

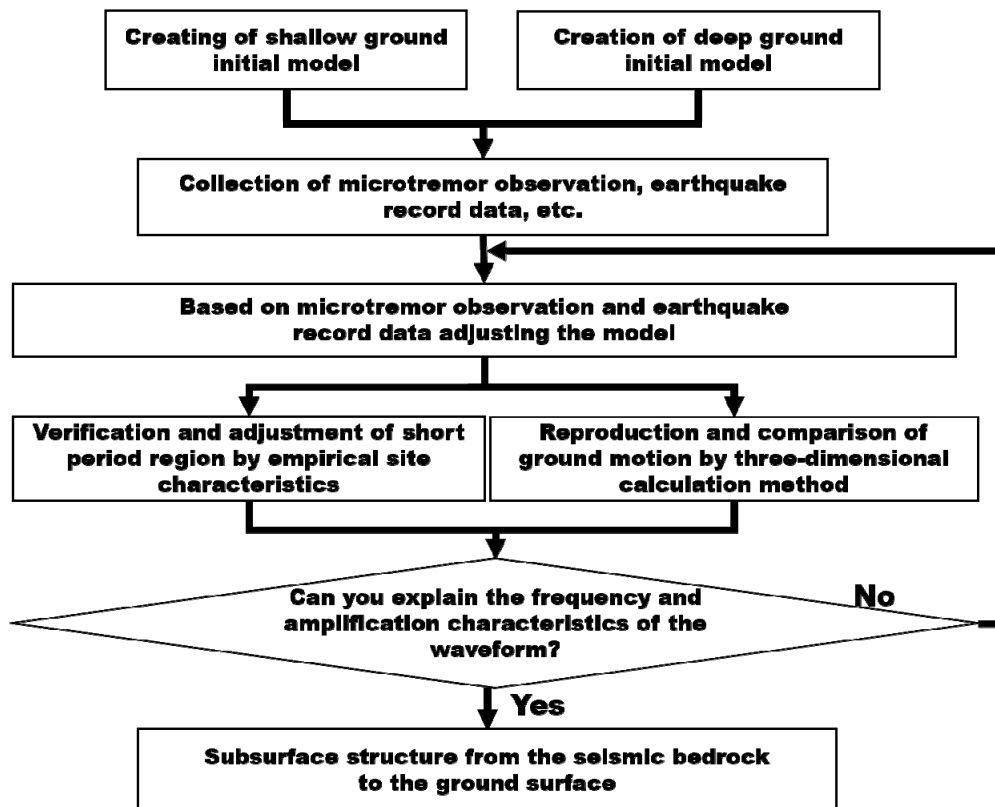


Fig. 2 – Process flow of shallow/deep-layers integrated ground modeling

3. Data collection for the ground structure modelling

In this study, for the whole Kanto area, we collected data such as boring data, ground motion records, and microtremor observations, as a fundamental information survey about the ground from the municipalities and other areas. For boring data collection, “Geo-Station” from NIED was used to convert publicly available data and newly collected data from municipalities and the private sector into XML format (digital data). They were used them mainly to make the shallow-layer model. For ground motion records, we collected observation records from K-NET, KiK-net, the Japan Meteorological Agency, and the municipalities (mainly prefectures). We collected data from April 1, 2001 to March 31, 2015. For microtremor observations, we conducted miniature array observations, which were mainly for a depth shallower than the engineering bedrock (shallow soil layers), and array observations for the seismic basement depth. Miniature array observations were done at about 13,000 points in public facilities and roads, and array observations were done at about 500 observation points for seismic intensity such as K-NET, KiK-net, and municipalities. In the observations, we used JU410 and JU215 (by Hakusan Corporation), which are integrated microtremor observation devices. In microtremor observations by miniature array[6], a regular triangle array with a 60 cm radius and an irregular triangle array with 5 to 15 m sides and no center point were placed with intervals of 1 to 2 km (Fig-3). The observation time of a miniature array was 15 minutes. During microtremor observations, arrays were set with an interval of about 5 km. Triangular arrays with radii (R) of 400 m, 200 m, and 100 m (an 800-meter array was also used in some areas) and L-shaped arrays with 75 m, 50 m, and 25 m sides were placed around seismometers from municipalities, K-NET, and KiK-net. We performed observations for 60 to 120 minutes using triangular arrays, depending on the radius of the array, and for around 30 minutes using small-size arrays such as L-shaped arrays.

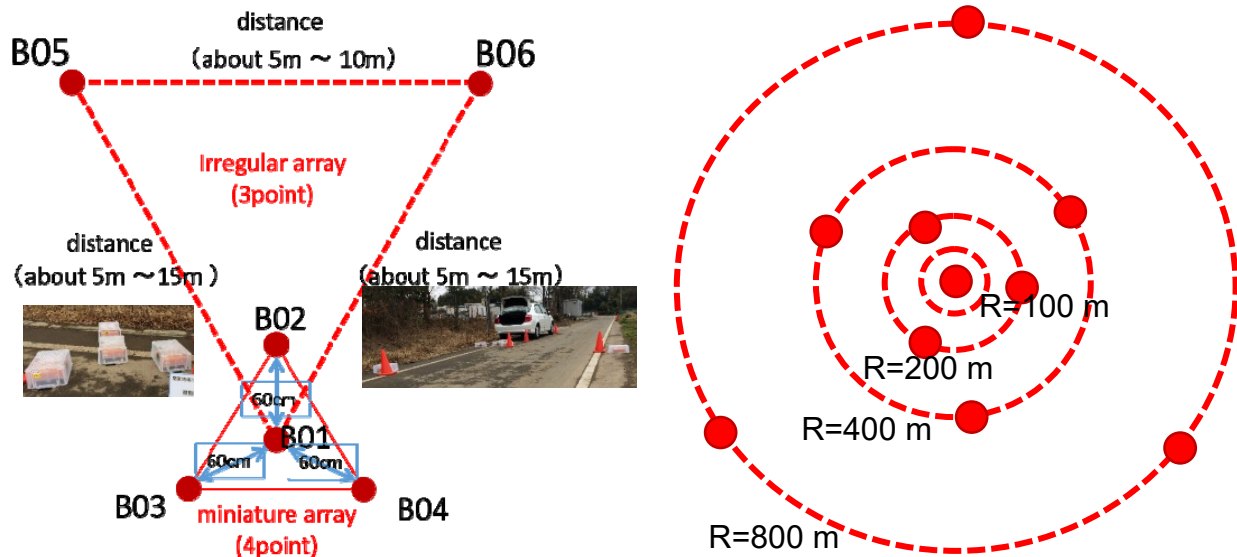


Fig.3 – Microtremor array observation

(Left: miniature array observation. Right: microtremor array observation)

4. Initial ground modelling (geologic model)

4.1 Shallow-layer model

The flow to make the shallow-layer model in this study is as follows.

- i) Set the stratigraphy for a target area, and classify columnar sections by geological feature.
- ii) Read the continuity of strata from each columnar section.
- iii) Make a geological structure model by interpolating stratum boundary data and assigning data into grids.
- iv) Convert N-values from the standard penetration test of boring data to S-wave velocities, and make the velocity structure model.

Fig.4 shows a distribution map of collected boring data. Note that in the interpolation mentioned in iii), we obtained stratum boundaries in all columnar sections to create layer structures by connecting these boundaries. We obtained the stratum boundary depth at the center of each grid in the ground model with a grid interval of about 250 m. Here, among various types of soil that constitute the stratum structure, we regarded the soil that accounts for the largest percentage as the soil that constitutes the stratum. For N-values, we obtained the representative value for each layer by the least squares method, then we derived the relational expression between N-values and S-wave velocities based on PS logging data, and we converted each layer to S-wave velocities. Fig.5 shows a conceptual diagram of the modeling method by spatial interpolation of analyzed ground structure data.

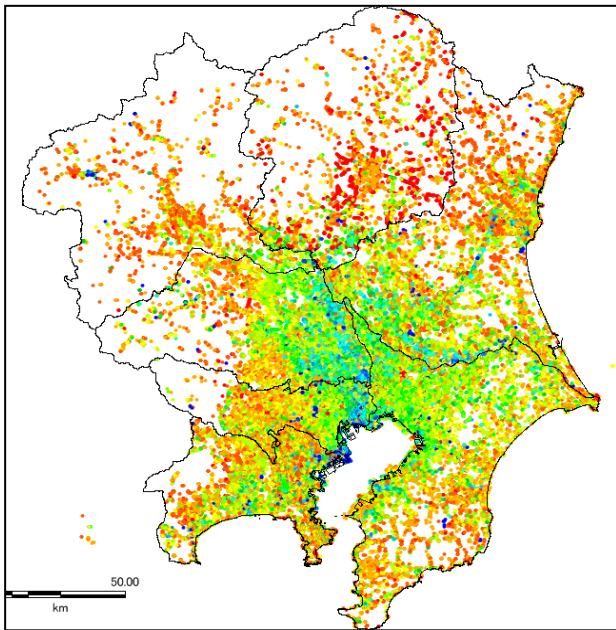


Fig.4 – Distribution map of boring data in the Kanto area (about 320,000 data)

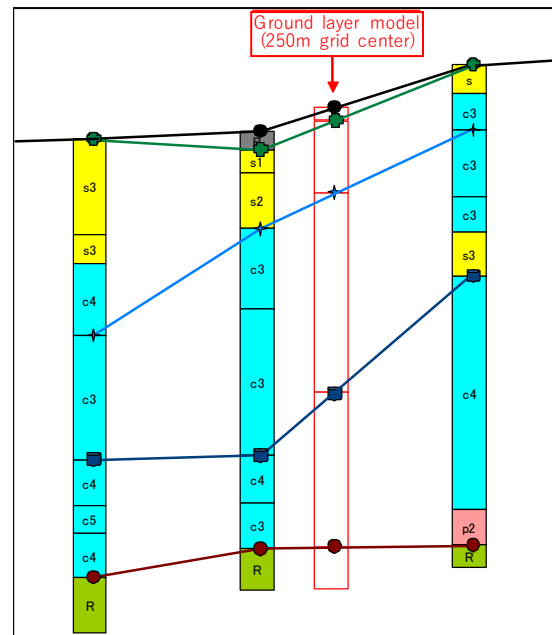


Fig.5 – Spatial interpolation of the shallow-layer modelling method

4.2 The deep-layer model and the initial shallow/deep-layers integrated ground model

For the deep subsurface structure model, we considered the already existent models and their evaluation for nationwide/broad areas. Therefore, in this study, we decided to use the national subsurface structure model (J-SHIS), which was made/evaluated consistently for nationwide areas. Combining the deep-layer model with the abovementioned shallow-layer model, shown in Section 4.1, we created the initial shallow/deep-layers integrated ground model. Fig.6 shows an example of the created model.

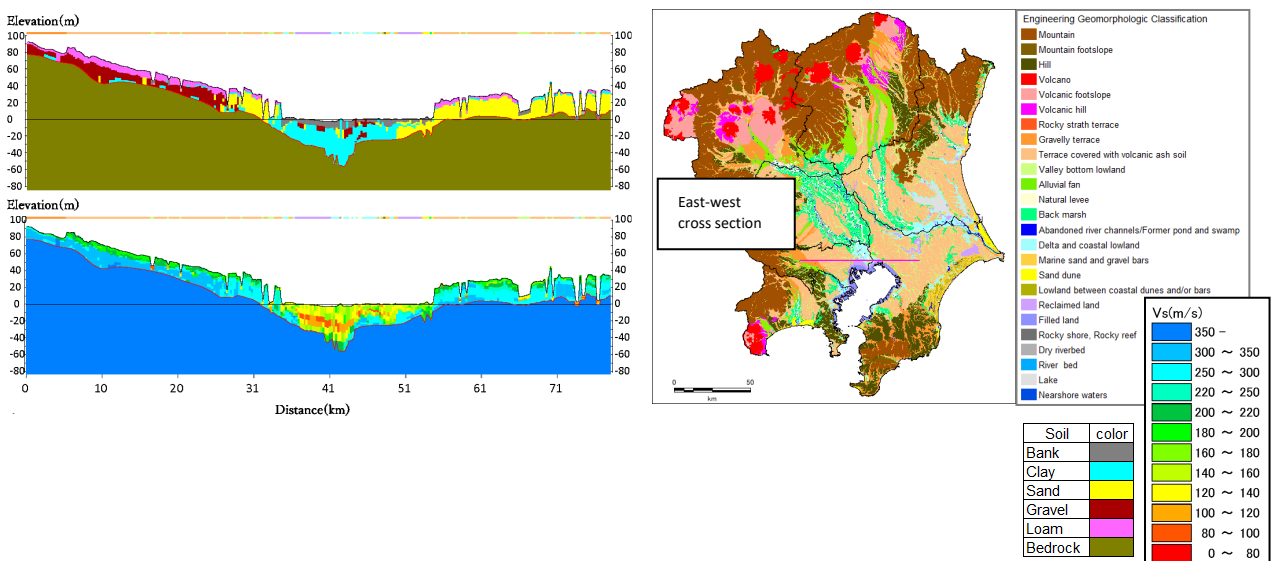


Fig.6 – Soil cross section and S-wave velocity cross section of the east-west cross-section



5. Correction analysis of the ground structure model

In microtremor surveys (arrays), we applied an inverse analysis method to measured dispersion curves generated from measurement data, and we obtained ground velocity structures. Note that for the inverse analysis, we obtained R/V spectra using the S-coda waves in seismic waveforms observed at nearby observation points of strong motion. Then, we performed joint inversion analysis in which the obtained R/V spectra were combined. For a method of joint inversion analysis, we referred to Arai and Tokimatsu (2004) [7] and Suzuki and Yamanaka (2011) [8]. Fig.7 shows the flow of the inverse analysis. Note that for the R/V spectrum ratio, we extracted waveforms after 20 seconds from the S-wave initial motion, and we obtained Fourier spectra of the radial component and the vertical-motion component. Then, we smoothed the spectra using Parzen window of 0.05 Hz bandwidth. We defined the phase velocity residuals and the R/V spectra in the joint inversion as follows.

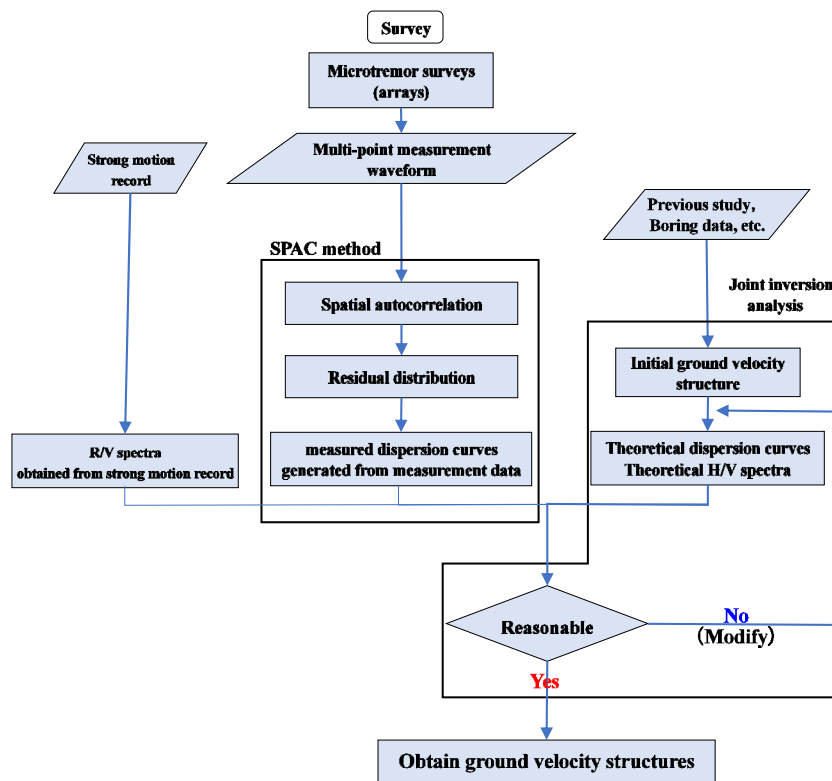


Fig.7 – Procedure of the joint inversion analysis for microtremor array and ground motion records

$$E_{PV} = \left(\frac{1}{N^{PV}} \sum_{j=1}^{N^{PV}} \left[w(f_j) \left(C^o(f_j) - C^c(f_j) \right) / C^o(f_j) \right]^2 \right) \quad (1)$$

$$w(f_j) = 1.0 (f_j > 1.0 \text{ Hz})$$

$$w(f_j) = f_j * 0.5 + 0.5 (f_j \leq 1.0 \text{ Hz}) \quad (2)$$

Here, N_{pv} , $C_o(f_j)$, $C_c(f_j)$ are the number of the phase velocity data, the measured phase velocity, and the theoretical phase velocity for a f_j frequency, respectively. $W(f)$ is a weighting function, and the larger the frequency, the larger the weight. In the same way, we defined the residual of the R/V spectra as follows.



$$E_{RV} = \left(\frac{1}{N_{RV}} \sum_{j=1}^{N_{RV}} \left[\frac{RV^O(f_j)}{RV_{max}^O} - \frac{RV^C(f_j)}{RV_{max}^C} \right] \right)^2 \quad (3)$$

Here, N_{RV} , $RV_o(f_j)$, $RV_c(f_j)$, RV_{max}^o , and RV_{max}^c are the number of the phase velocity data, the observed R/V spectrum and the theoretical H/V spectrum for a frequency f_j , the maximum value of the observed R/V spectra, and the maximum value of the theoretical H/V spectra, respectively. Using these residuals, we defined the residual of the whole observation data as follows.

$$E = 0.5E_{PV} + 0.5E_{RV} \quad (4)$$

An example of the joint inversion correction result is shown in Fig.8.

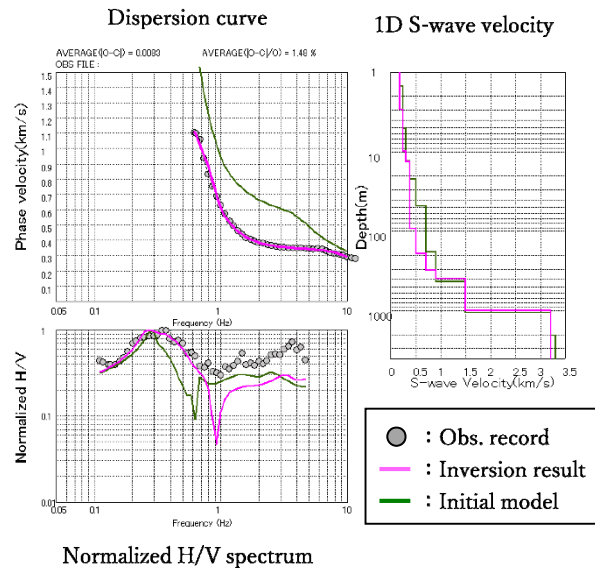


Fig.8 – Example of the joint inversion correction result
(General branch office at Asahi, Chiba)

6. Accuracy verification of the ground structure model

6.1 Site amplification factors

To estimate the site amplification factors at the observation points, we used data from K-NET and KiK-net for the Kanto area, and seismometer data for municipalities. We used ground motion records of medium-scale earthquakes between M5 to M6 observed mainly in Chiba and Ibaraki Prefectures. Earthquakes whose focal depths were 40 km and over and focal distances within 50 km were selected. In the spectral inversion analysis, referring to Kataoka et al. (2006) [9], we obtained the seismic source spectra and used a model with ω^2 . In addition to that, because of the constraint conditions to obtain the site amplification factors, we had to identify S-wave velocity structures, and to determine the spectrum ratios between the surface seismometer



and the underground seismometers at six points in Narita (CHBH13), Juo (IBRH14), and Tsukuba (IBRH19). Fig.9 and Table 1 show epicenter locations for the analyzed earthquakes, comparisons of moments with those obtained in F-net, and Q-values in various propagation paths.

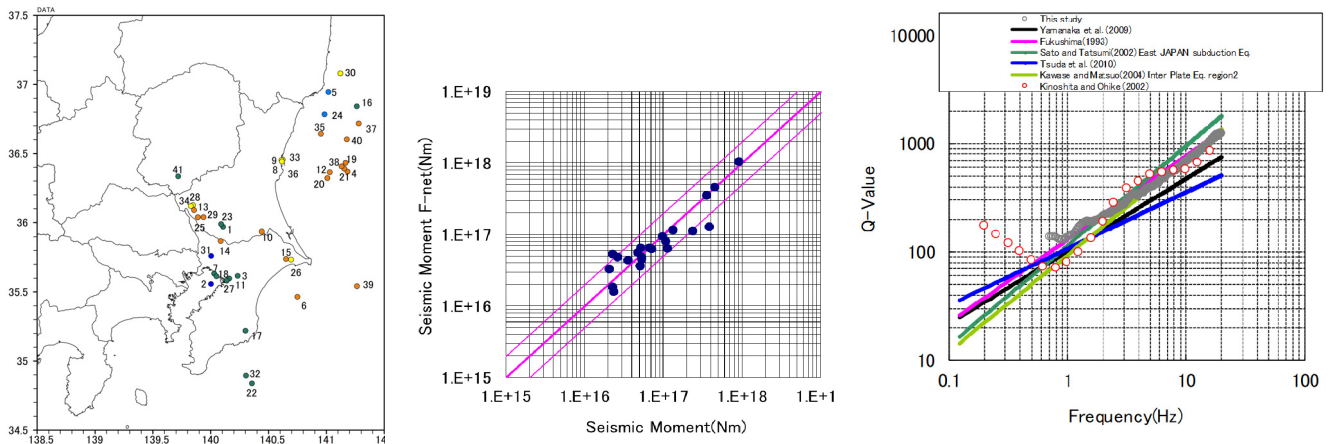


Fig.9 – Epicenter locations obtained by spectrum inversion (left), comparison of seismic moments using F-net (middle), and Q-values in various propagation paths (right)

Table1 – List of analyzed seismic focuses

No	Date	Hour	Minutes	Latitude	Longitude	Depth(km)	Mj	Mo(Nm)	Epicenter
1	1997/3/23	14	58	35.9687	140.1070	71.46	5.1	4.77E+16	SOUTHERN IBARAKI PREF
2	1997/9/8	8	40	35.5560	140.0022	108.59	5.1	6.62E+16	CENTRAL CHIBA PREF
3	1998/1/14	2	17	35.6165	140.2328	77.98	5.0	2.28E+16	CENTRAL CHIBA PREF
4	1998/3/23	18	37	36.3690	141.1820	48.60	5.4	1.28E+17	E OFF IBARAKI PREF
5	1998/4/9	17	45	36.9452	141.0172	94.87	5.4	1.78E+17	E OFF FUKUSHIMA PREF
6	1998/6/14	22	17	35.4645	140.7490	46.43	5.7	3.58E+17	KUJUKURI COAST BOSO PEN
7	1998/8/29	8	46	35.6330	140.0293	64.60	5.3	9.80E+16	CENTRAL CHIBA PREF
8	1999/3/26	8	31	36.4507	140.6155	59.04	5.0	4.55E+16	NORTHERN IBARAKI PREF
9	1999/4/25	21	27	36.4560	140.6220	59.47	5.2	6.24E+16	NORTHERN IBARAKI PREF
10	1999/7/15	7	56	35.9357	140.4410	49.64	5.0	5.33E+16	SOUTHERN IBARAKI PREF
11	1999/9/13	7	56	35.5977	140.1598	75.81	5.1	1.08E+17	CENTRAL CHIBA PREF
12	2003/1/21	13	19	36.3645	141.0290	46.62	5.1	4.60E+16	E OFF IBARAKI PREF
13	2003/3/13	12	12	36.0902	139.8557	47.26	5.0	2.34E+16	SW IBARAKI PREF
14	2003/5/12	0	57	35.8688	140.0857	46.87	5.3	7.07E+16	SOUTHERN IBARAKI PREF
15	2003/5/17	23	33	35.7385	140.6507	47.29	5.3	1.13E+17	NEAR CHOSHI CITY
16	2003/6/16	18	34	36.8415	141.2623	76.92	5.1	2.48E+16	E OFF IBARAKI PREF
17	2003/9/20	12	54	35.2188	140.3003	69.96	5.8	3.53E+17	KUJUKURI COAST BOSO PEN
18	2003/10/15	16	30	35.6137	140.0498	73.90	5.1	5.15E+16	CENTRAL CHIBA PREF
19	2003/11/15	3	43	36.4325	141.1652	48.40	5.8	3.43E+17	E OFF IBARAKI PREF
20	2004/3/11	11	34	36.3220	141.0082	47.52	5.3	1.04E+17	E OFF IBARAKI PREF
21	2004/4/4	8	2	36.3902	141.1540	48.99	5.8	8.38E+17	E OFF IBARAKI PREF
22	2004/7/17	15	10	34.8382	140.3560	68.68	5.5	2.39E+17	SE OFF BOSO PENINSULA
23	2004/10/6	23	40	35.9888	140.0898	65.97	5.7	4.52E+17	SOUTHERN IBARAKI PREF
24	2005/1/1	5	13	36.7835	140.9833	89.42	5.0	3.64E+16	E OFF IBARAKI PREF
25	2005/2/16	4	46	36.0385	139.8888	46.15	5.3	1.33E+17	SW IBARAKI PREF
26	2005/6/20	1	15	35.7338	140.6947	50.65	5.6	3.81E+17	NEAR CHOSHI CITY
27	2005/7/23	16	34	35.5817	140.1385	73.08	6.0	9.11E+17	CENTRAL CHIBA PREF
28	2005/7/28	19	15	36.1262	139.8463	51.12	5.0	2.28E+16	SW IBARAKI PREF
29	2005/10/16	16	5	36.0393	139.9375	47.12	5.1	3.57E+16	SW IBARAKI PREF
30	2005/10/22	22	12	37.0797	141.1205	51.96	5.6	2.06E+17	E OFF FUKUSHIMA PREF
31	2006/2/1	20	35	35.7610	140.0037	101.02	5.1	5.07E+16	NORTHERN CHIBA PREF
32	2006/10/14	6	38	34.8948	140.3048	64.42	5.1	2.62E+16	SE OFF BOSO PENINSULA
33	2008/3/8	1	54	36.4525	140.6117	57.04	5.2	5.57E+16	NORTHERN IBARAKI PREF
34	2008/4/4	19	1	36.1200	139.8282	53.48	5.0	2.05E+16	SW IBARAKI PREF
35	2008/7/5	16	49	36.6427	140.9520	49.69	5.2	5.25E+16	E OFF IBARAKI PREF
36	2008/8/22	19	59	36.4418	140.6153	55.92	5.2	5.02E+16	NORTHERN IBARAKI PREF
37	2009/2/1	6	51	36.7170	141.2793	47.03	5.8	4.65E+17	E OFF IBARAKI PREF
38	2009/4/28	6	37	36.4070	141.1307	47.88	5.0	5.80E+16	E OFF IBARAKI PREF
39	2009/6/6	14	52	35.5418	141.2642	42.40	5.9	5.48E+17	NEAR CHOSHI CITY
40	2009/10/23	10	28	36.6023	141.1762	45.15	5.0	1.67E+16	E OFF IBARAKI PREF
41	2009/12/18	5	41	36.3347	139.7190	78.05	5.1	5.31E+16	SOUTHERN TOCHIGI PREF

6.2 Q-values

We estimated the Q-value by comparing the estimated observed amplification factor and the theoretical amplification factor. We introduced a bilinear-type Q-value as shown in Eq.(5). The value of f_c was fixed as 5 Hz, referring to Fukushima and Midorikawa (1994) [10], and the values of a and b were fixed as 10.6 and 0.44, respectively, referring to Yamanaka et al. (2009) [11].



$$Q(f) = \frac{V_S}{a} \cdot f_c^b (f \geq f_c) \quad Q(f) = \frac{V_S}{a} \cdot f^b (f < f_c) \quad (5)$$

Here, V_S is the S-wave velocity (m/s) of each layer, and f is a frequency (Hz). We show calculated seismic source spectra. From the comparison between seismic moments and F-net values shown in Fig.9, we see that data are mostly distributed between 0.5 to 2 times the original values compared with those in F-net. For Q-values in propagation paths, the results are almost consistent with those in Yamanaka et al. (2010) for frequency 4 Hz and over. Compared with results in existing studies (for example, reference[11]), the results are not significantly different. Fig.10 shows the calculated spectrum amplification factors. As a reference of the comparison of the site amplification factors, we compared the data with the results in Nozu and Nagao (2006) [12], and our results are generally consistent with theirs.

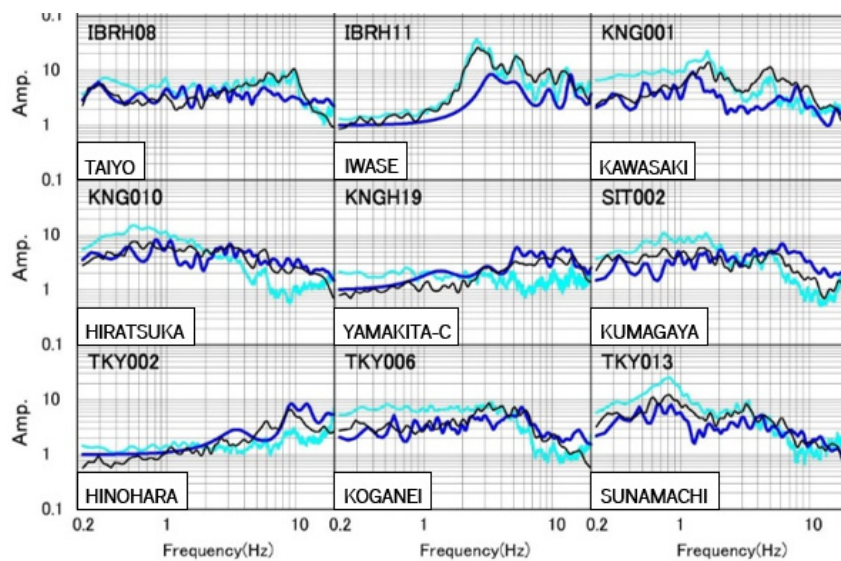


Fig.10 – Observed amplification factors (black), amplification factors by the ground model (blue), spectrum amplification factors by Nozu and Nagao (2005) (light blue)

6.3 Three-dimensional finite difference method

Using the corrected shallow/deep-layers integrated ground structure model, we performed ground motion simulations by finite difference method, then, we verified the model by reproducing long-period components. For verification periods longer than one second, the velocity $V_S = 350$ m/s was calculated as the engineering bedrock, without using the shallow-layer ground structure model. Note that for the observed seismic waveforms, which provide the target data for the comparison, we performed a treatment to return those waveforms to the upper layer with $V_S = 350$ m/s, using the one-dimensional multiple reflection method based on the shallow-layer ground structure model. From Table 2, we can see the physical property values of the shallow/deep-layers integrated ground structure model, which we used for this examination. For finite difference computation, we generated finite difference grids with an interval of 70 m in the horizontal direction \times 35 m in the vertical direction (Table 3). The Q-value is basically 1/5 of the S-wave velocity, and the reference period of 3 seconds was used. The target earthquakes for calculation are five hypocenters shown in Fig.11, and we output waveforms at 197 observation points in K-NET and KiK-net at Ibaraki, Chiba, Tochigi, Gunma, Saitama, Tokyo, and Kanagawa Prefectures. We corrected the observation records that we used for the comparison using the one-dimensional multiple reflection method based on the shallow-layer ground model in the shallow/deep-layer integrated ground model, then, they were evaluated on the open engineering bedrock. To evaluate the results from the finite difference method, we used goodness-of-fit (GOF) and combined GOF (CGOF) (Dreger et al., (2015) [13]) as index values to evaluate the



reproducibility of the computation record (model) for the observation record (data). GOF and CGOF are expressed by the following equation (Eq.(7)).

$$\text{GOF} = \ln(\text{data}/\text{model}) \quad (6)$$

$$\text{CGOF} = \frac{1}{2} \left\langle |\ln(\text{data}/\text{model})| \right\rangle + \frac{1}{2} \left\langle |\ln(\text{data}/\text{model})| \right\rangle^2 \quad (7)$$

The first term in the right side of Eq.(7) expresses the absolute value of the mean GOF. The second term is the mean of the absolute values (in other words, the mean and the variance). To calculate the index values, we used the vector composition value of the two horizontal components of the Fourier spectrum. In the deep-layer ground structure model, although the depth structure of the layer corresponding to the seismic basement ($V_s = 3200$ m/s) is not significantly different from that in existing models, we performed an evaluation by adding a layer with $V_s = 350$ m/s, which is the layer corresponding to the engineering bedrock, important for widening the bandwidth. Due to this addition of the layer, each layer of $V_s = 500\sim 900$ m/s is substantially corrected, and periods and amplification factors show good agreement in periods larger than 2 seconds (Fig.12).

Table 2 – Physical property values of the subsurface structure model used in this examination (Yellow hatch are physical-properties value of the Kanto district)

Layer	$V_s(\text{km/s})$	$V_p(\text{km/s})$	$\rho(\text{g/cm}^3)$
1	0.35	1.6	1.85
2	0.40	1.6	1.85
3	0.45	1.7	1.90
4	0.50	1.8	1.90
5	0.55	1.8	1.90
6	0.60	2.0	1.90
7	0.65	2.0	1.95
8	0.70	2.1	2.00
9	0.75	2.1	2.00
10	0.80	2.2	2.00
11	0.85	2.3	2.05
12	0.90	2.4	2.05
13	0.95	2.4	2.10
14	1.0	2.5	2.10
15	1.1	2.5	2.15
16	1.2	2.6	2.15
17	1.3	2.7	2.20
18	1.4	3.0	2.25
19	1.5	3.2	2.25
20	1.6	3.4	2.30
21	1.7	3.5	2.30
22	1.8	3.6	2.35
23	1.9	3.7	2.35
24	2.0	3.8	2.40
25	2.1	4.0	2.40
26	2.1	4.0	2.40
27	2.7	5.0	2.50
28	2.9	4.6	2.55
29	2.7	5.0	2.50
30	3.1	5.5	2.60
31	3.2	5.5	2.65

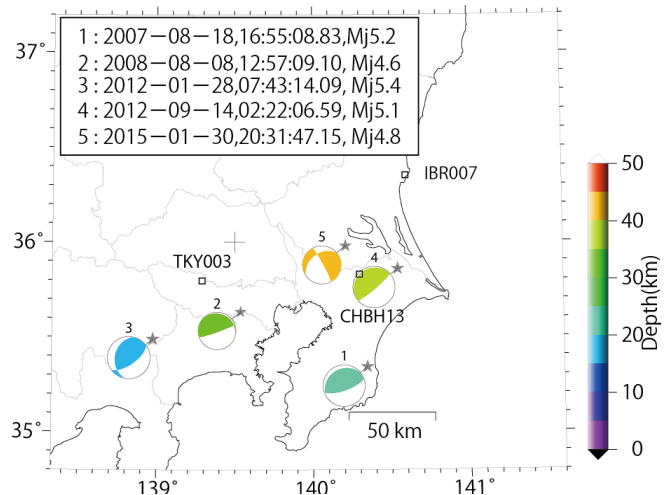


Fig.11 – Earthquakes used for the calculation

Table 3 – Overview of the calculation

Structure model					
Grid size (m)					
First domain					
dx1	dy1		dz1		
70	70		35		
Number of grids (in the second domain, the number is three times larger than in the first domain)					
First domain			Second domain		
nx1	ny1	nz1	nx2	ny2	nz2
3789	4146	231	1263	1382	400
Calculation time interval (second)					
0.003125					

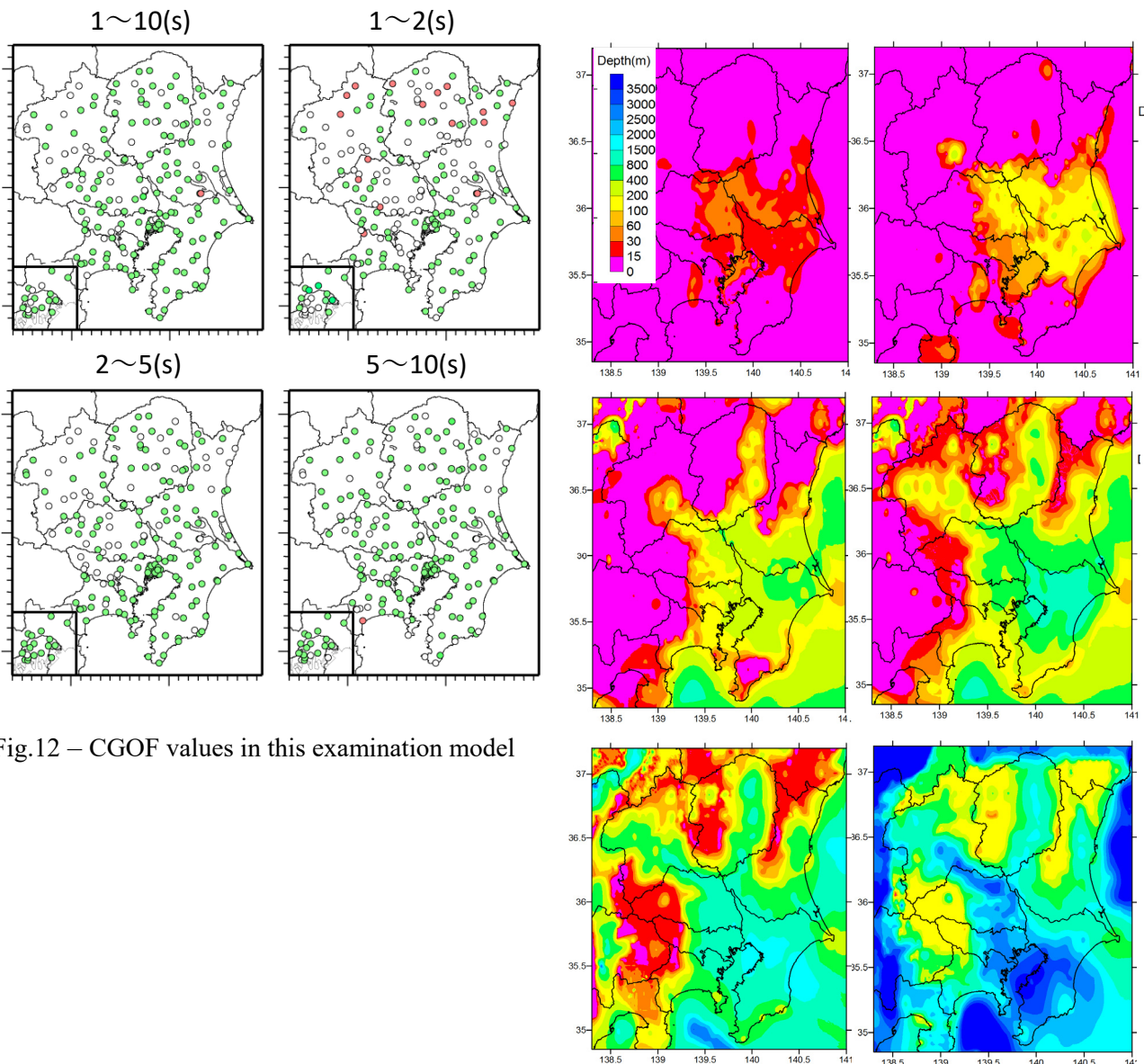


Fig.12 – CGOF values in this examination model

Fig.13 – Top surface depth of the S-wave velocity layer in the deep-layer ground of the shallow/deep-layers integrated ground structure model (from the upper left, $V_s = 350\sim 500$ m/s; from the middle left, $V_s = 700\sim 900$ m/s; from the lower left $V_s = 1500\sim 3200$ m/s). The legends for contour colors and depths are shown in upper right.

7. Conclusions

In this study, starting from a geologic model, we developed a shallow/deep-layers integrated ground model using microtremor array surveys and microtremor measurement results. In addition, we verified the time accuracy through amplification factors of the created shallow/deep-layers integrated ground model. As a general tendency, the accuracy for long-time results for the whole broadband range were improved, for example, we can say that the results for periods near 1 second and periods longer than that, which are important from a viewpoint of disaster prevention, have substantially improved. We consider that this result is not only because the shallow-layer model has been elaborated by the collection of boring columnar sections, but also because of the high accuracy of structures around the engineering bedrock with $V_s =$



300~700 m/s, which connects the shallow layers and deep layers. Since the initial ground structure used this method, the velocity structure model particularly around the engineering bedrock was stably improved in all areas, even in locations where it is hard to make the initial ground structure due to the collection density of boring data. At this time, we have already modelled 1/4 of Japan, including the Kanto, Tokai, and Kumamoto areas, through the method in this study. We plan to expand the modeling nationwide in the future.

References

- [1] Miyake H, Koketsu K, Furumura T, Inagaki Y, Masuda T, Midorikawa S. Integration of the shallow subsurface-structure model for strong ground motion prediction in the Tokyo metropolitan area (in Japanese), Proceedings of the 12th Japan Earthquake Engineering Symposium, pp.214-217, 2006.
- [2] H. Fujiwara et al., "A Study on Subsurface Structure Model for Deep Sedimentary layers of Japan for Strong-motion Evaluation," Technical Note of NIED, No.337, 2009 (in Japanese).
- [3] Aoi, S. and H. Fujiwara : 3-D finite-difference method using discontinuous grids, Bull. Seismol. Soc. Am., **89**, pp.918-930, 1999.
- [4] Senna, S., T. Maeda, Y. Inagaki, H. Suzuki, N. Matsuyama, and H. Fujiwara : Modeling of the subsurface structure from the seismic bedrock to the ground surface for a broadband strong motion evaluation, Journal of Disaster research., Vol.8, No.5, pp.889-903, 2013.
- [5] S. Senna, A. Wakai, H. Suzuki, A. Yatagai, H. Matsuyama, and H. Fujiwara, "Modeling of the Subsurface Structure from the Seismic Bedrock to the Ground Surface for a Broadband Strong Motion Evaluation in Kumamoto Plain," *J. Disaster Res.*, Vol.13, No.5, pp. 917-927, 2018.
- [6] Cho I, Senna S, Fujiwara H., Miniature array analysis of microtremors, Geophysics, 78, KS13-KS23, doi:10.1190/geo2012-0248.1, 2013.
- [7] Arai, H., and K. Tokimatsu : S-Wave velocity profiling by inversion of microtremor H/V Spectrum, Bull. Seismol. Soc. Am., 94, pp.53-63, 2004.
- [8] Haruhiko Suzuki, Hiroaki Yamanaka : Joint inversion using earthquake ground motion records and microtremor survey data to S-wave profile of deep sedimentary layers, Japan Geophysics, 63, pp.215-227, 2010.
- [9] Kataoka S, Sato T, Matsumoto S, Matsumoto T., Attenuation Relationships of Ground Motion Intensity Using Short Period Level as a Variable (in Japanese), Journal of JSCE, A62(4), pp.740-757, 2006.
- [10] Fukushima Y, Midorikawa S : PREDICTION OF VELOCITY RESPONSE SPECTRA FOR SEISMIC MOTIONS IN AND ON ROCK SITE CONSIDERING NONLINEAR SCALING OF M_w^2 TERM ; Journal of Struct Constr Engng, AIJ, 447, pp.39~49, 1993.
- [11] Yamanaka H, Ohori M, Midorikawa S. 21024 Estimation of seamless V_s structure for Kanto basin using site amplification from spectral inversion of earthquake motion records (in Japanese), Summaries of technical papers of annual meeting Architectural Institute of Japan, B-2, StructureII , pp.47-48, 2010.
- [12] A.Nozu and T.Nagao, "Site amplification factors for strong-motion sites in Japan based on spectral inversion technique," PARI Technical Note, No.1112, 2005 (in Japanese).
- [13] Dreger, D. S., G. C. Beroza, S. M. Day, C. A. Goulet, T. H. Jordan, P. A. Spudich, and J. P. Stewart, Validation of the SCEC broadband platform V14.3 simulation methods using pseudospectral acceleration data, *Seismol. Res. Lett.*, **86**, 39–47, 2015.